Charge transfer and weak chemisorption of oxygen molecules in nanoporous carbon consisting of a disordered network of nanographene sheets

2010 J. Phys.: Condens. Matter 22 334208

(http://iopscience.iop.org/0953-8984/22/33/334208)

J. Phys.: Condens. Matter **22** (2010) 334208 (8pp) doi:10.1088/0953-8984/22/33/334208

Charge transfer and weak chemisorption of oxygen molecules in nanoporous carbon consisting of a disordered network of nanographene sheets

G U Sumanasekera[1,3], G Chen[1,4], K Takai[2], J Joly[2], N Kobayashi[2], T Enoki[2] and P C Eklund[1]

[1] Department of Physics, Pennsylvania State University, University Park, PA 16802, USA
[2] Department of Chemistry, Tokyo Institute of Technology, Ookayama, Meguro, Tokyo, 152-8551, Japan

Received 22 December 2009, in final form 8 February 2010
Published 4 August 2010
Online at stacks.iop.org/JPhysCM/22/334208

Abstract

The adsorption/desorption processes of oxygen are investigated in nanoporous carbon (activated carbon fiber (ACF)) consisting of a disordered network of nanographene sheets. The heat-induced desorption at 200 °C shows the decomposition of oxygen-including functional groups weakly bonded to nanographene edges. The removal of these oxygen-including negatively charged functional groups brings about a change in the type of majority carriers, from holes to electrons, through charge transfer from the functional groups to the interior of nanographene sheets. The oxygen adsorption brings ACF back to the electronic state with holes being majority carriers. In this process, a large concentration of negatively charged $O_2^{\delta-}$ molecules with $\delta \sim 0.1$ are created through charge transfer from nanographene sheets to the adsorbed oxygen molecules. The changes in the thermoelectric power and the electrical resistance in the oxygen desorption process is steeper than that in the oxygen adsorption process. This suggests the irreversibility between the two processes.

(Some figures in this article are in colour only in the electronic version)

1. Introduction

It is well known that carbon-based materials can act as a host for the adsorption of guest materials. Activated carbon, which is one of the most important materials among these, accommodates a huge amount of guest materials physisorptively in micropores surrounded by disordered graphitic structures [1–4]. In these materials, not only the pores but also graphene edges can cause the adsorption activity [5]. Bulk graphite is also among the important materials in which the amphoteric nature inherent to the semimetallic or zero-gap semiconductive electronic structure works to create graphite intercalation compounds with a huge variety of guest species [6]. Here, donor/acceptor species are accommodated into the graphitic galleries through charge transfer interaction between the host graphite and guest species; charge is transferred from/to graphite to/from the guest species when the guest is an acceptor/donor. From the observations on the guest adsorption phenomena in this variety of carbon-based materials, depending on the type of host and guest materials, there are a wide range of interactions from weak van der Waals, charge transfer, even to covalent bonding, which are responsible for the adsorption of guest species. Accordingly, a wide range of guest species having different electronic characteristics can participate in the adsorption/reaction with carbon-based materials.

In particular, the oxygen molecule, which we focus on in the present paper, is situated at a unique position in the host–guest interaction with graphitic materials. A rough overview of the activities of oxygen molecules as guest species can be summarized simply in the following way. Oxygen molecules are physisorbed on the surface

[3] Present address: Department of Physics and Astronomy, University of Louisville, Louisville, KY 40292, USA.
[4] Present address: Honda Research Institute USA Inc, Columbus, OH 43212, USA.

and edges of a graphene sheet at low temperatures. When the temperature is elevated, an oxygen molecule reacts with the edges of the graphene sheet. A further increase in the temperature brings about the oxidation of graphene edges after the oxygen molecules are dissociated. However, the details have not been clarified well for the adsorption/reaction of oxygen molecules with the graphitic carbon host. Indeed, the electronegativity of oxygen molecules is expected to act seriously in the adsorption/reaction process, resulting in the participation of charge transfer in the adsorption state, although the electronegativity is not strong enough to bring about an intercalation reaction. In addition, the magnetic degree of freedom of an oxygen molecule having a triplet spin state ($S = 1$) is considered to play an important role in the adsorption [7, 8].

In the present paper, we report the oxygen adsorption mechanism in activated carbon fibers (ACFs), which are nanographene-based nanoporous carbon having a uniform distribution of nanopores with huge specific surface areas of 1500–3000 $m^2\ g^{-1}$ [2, 3, 9–13]. The structure of ACFs consists of a three-dimensional disordered network of nanographite domains, each of which is a stack of 3–4 nanographene sheets having a mean in-plane size of ca. 3 nm. We investigated the oxygen adsorption effect on the electrical resistivity, thermoelectric power (TEP), and Raman spectra, which were sensitive to the charge transfer interaction. The homogeneity of the nanopore distribution and nanographite sizes with well defined nanographene sheets allows us to get detailed information on the interaction between adsorbed oxygen molecules and nanographite.

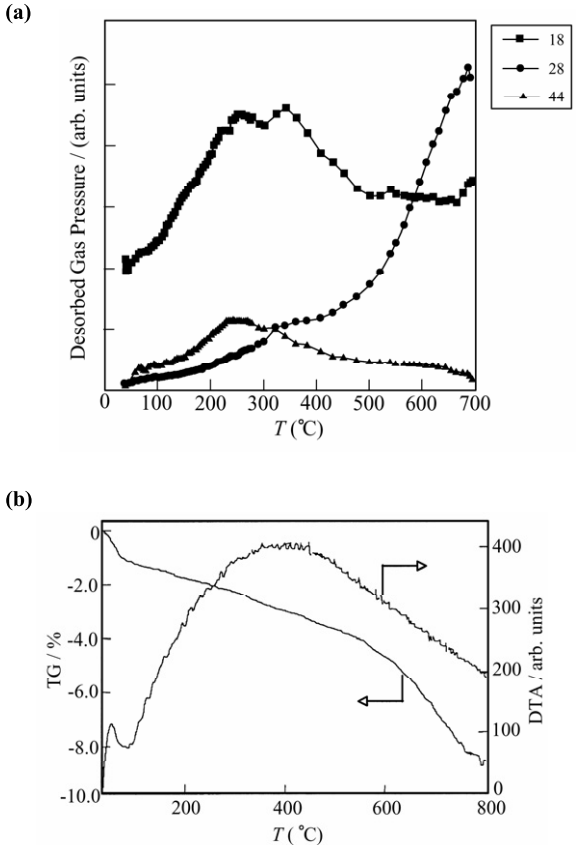

Figure 1. (a) TPD spectra for mass numbers of 18, 28 and 44, which correspond to H_2O, CO and CO_2, respectively. (b) TG and DTA traces as a function of T.

2. Experimental details

In this study we used commercially available ACFs (FR20, Kurarey Chemical Co.) having been prepared by activation of phenol-based precursor materials at 800–1200 °C in an atmosphere of CO_2 and H_2O. They show specific surface areas (SSA) of ∼2000 $m^2\ g^{-1}$. Temperature programmed desorption (TPD) and thermogravimetric (TG)/differential thermal analysis (DTA) measurements were carried out in the temperature ranges up to 700 °C with a heating rate of 4 °C min^{-1} in vacuum, and up to 800 °C with a heating rate of 10 °C min^{-1} in an Ar atmosphere, respectively, in order to clarify the effect of heat treatment on the ACF samples. The sample for TPD was evacuated at 1×10^{-6} Torr for 2 h prior to the measurement. The electrical transport measurements were carried out for a single fiber along its fiber axis. Two Chromel/Au-7 at.%Fe thermocouple junctions were attached to the ends of the fiber with silver epoxy. Two additional Cu leads (all 0.003 in dia. wires) were attached between the thermocouple junctions, in equal spacing, to measure the thermoelectric power (TEP) [14] and four-probe electrical resistance. A platinum resistor thermometer attached to one end of the fiber was used to maintain a temperature gradient of ∼1 K along the fiber axis. The TEP was measured using an analog-subtraction technique [14, 15]. The sample was placed in an apparatus for *in situ* studies so that it could be heated or cooled (4 K $< T <$ 600 K). The sample cell was evacuated using a turbo molecular pump.

Raman scattering experiments with a laser excitation of 488 nm were carried out in a backscattering geometry in an optical cell, equipped with a sapphire window, that could be pressurized to ∼4 atm or evacuated. The free O_2 molecule band was observed by admitting O_2 at 80 K (below the boiling point (90 K) of O_2). For faster kinetics, O_2 was admitted at 350 K with an overpressure of 4 atm and quenched to 80 K. Then, while evacuating the sample using a turbo molecular pump, spectra were recorded on a warming cycle from 80 to 300 K.

3. Results

Figures 1(a) and (b) show the results of the TPD and TG/DTA measurements in the temperature ranges up to 700 °C and 800 °C, respectively. Mass peaks of 18, 28 and 44 are observed as the main desorbed gaseous species, accompanied by other weak peaks whose intensities are a little bit larger than the fluctuations of the background. The masses of 18, 28 and 44 are assigned to H_2O, CO and CO_2 desorbed after the heat-induced decomposition of functional groups bonded to the edge carbon atoms, in addition to the physisorbed species appearing in the low temperature regime. According to the results, the H_2O peak appears over the entire temperature

regime investigated. The H_2O peak is higher than the peaks of CO and CO_2, except above 600 °C, and the CO peak is the lowest at room temperature. The H_2O peak is high even at room temperature. It increases gradually with a double peaked feature around 250–350 °C, decreases above the feature as the temperature is elevated up to 500 °C, and shows a plateau in the temperature range of 500–650 °C. The CO peak, which is very small at room temperature, gradually increases as the temperature is elevated up to 320 °C, around which it has a plateau. After that, it increases again and the slope becomes steep as the temperature rises. Interestingly, the temperature of the plateau is almost the same as the temperature at which the H_2O peak shows a second peak. The CO_2 peak increases upon the elevation of the temperature up to 250 °C, and then it declines monotonically above that temperature. The temperature (250 °C) of this peak is coincident with that of the first peak of H_2O.

Figure 1(b) shows the TG and DTA traces. The TG trace shows a steep decrease with the temperature up to 50 °C, and then a moderate decrease in further elevation of the temperature up to 600 °C. The weight change up to 50 °C, which corresponds to the amount of adsorbed foreign gas species, is ca. 1.5%. Above 600 °C, the slope of the trace becomes steep again. The low temperature steep decrease in TG, which corresponds to the appearance of a peak in the DTA at around 30 °C, is associated with the desorption of ambient gas species weakly adsorbed in the nanopores.

The results of the TPD and TG/DTA measurements tell us what the adsorbed species and functional groups bonded to the edge carbon atoms are. The desorption of H_2O taking place at temperatures up to ca. 50 °C is naturally assigned to H_2O molecules physisorbed to the nanopores. Following the desorption of the physisorbed foreign species, mainly water, from the nanopores, the decomposition of functional groups results in the desorbed species, the majority of which are H_2O, CO and CO_2. The functional groups are oxygen-including chemical species produced in the oxidation process of the nanographene edges. The oxidation of the nanographene edges is considered as creating typically carboxyl (–COOH), carbonyl (>C=O), and phenol (–OH) groups [4]. The steep growth of the CO_2 peak, together with the increase in the H_2O peak, in the temperature range up to ca. 250 °C is associated with the decomposition of carboxyl groups. The growth of the CO peak, which occurs at temperatures after the CO_2 and H_2O peaks have peaked, consists in the decomposition of carbonyl and phenol groups, which are more strongly bonded to the edge carbon atoms.

Figure 2 shows the kinetics of oxygen adsorption and desorption on a single ACF at 200 °C, as observed with (a) TEP (S) and (b) electrical resistance change (R). The experiment was carried out as follows: the sample was first heated up to 200 °C and then evacuated to investigate the desorption process. After we achieved the equilibrium state around 36 h, 1 atm of oxygen gas was introduced for the adsorption process. The gas pressure and temperature stabilized to equilibrium values within a few minutes after the introduction of oxygen gas. The change in the TEP and electrical resistance were tracked in these desorption/adsorption processes. The TEP

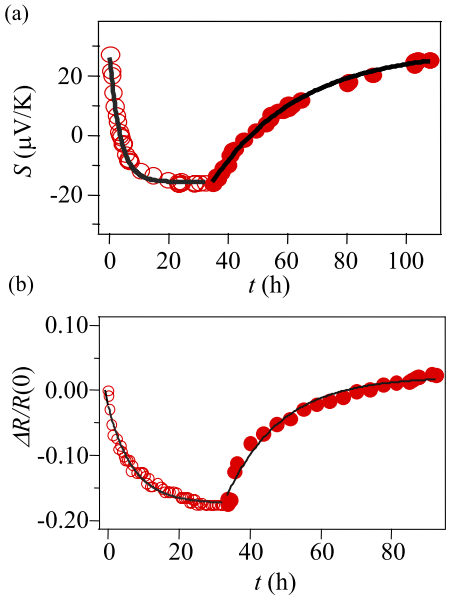

Figure 2. Kinetics of oxygen adsorption and desorption on a single ACF at 200 °C, as observed with (a) TEP (S) and (b) change in resistance (ΔR). The open and closed circles denote the data for the desorption and adsorption processes, respectively. The change ΔR of the resistance with respect to the initial value is plotted. Evacuating of the sample started at 0 h, and 1 atm of oxygen was introduced at 36 h. The solid lines are fits with relaxation times of the desorption and adsorption processes; $\tau_{Sd} = 3.2$ and $\tau_{Sa} = 26.7$ h, respectively, for the thermoelectric power, and $\tau_{Rd} = 6.2$ and $\tau_{Ra} = 12.3$ h, respectively, for the electrical resistance change.

decreases exponentially just after the evacuation of the sample starts. It reaches the steady state in ca. 20 h. Interestingly, the sign of the TEP changes from positive to negative in the evacuation process, suggesting a change in the majority carriers from holes to electrons. The introduction of oxygen gas makes the TEP increase exponentially. It achieves the steady state in ca. 60 h after the introduction of oxygen gas. The sign of the TEP changes back from negative to positive. This suggests that the oxygen works to create hole carriers. The electrical resistance shows an exponential change in the desorption and adsorption processes. The resistance decreases in the evacuation process, while it increases in the oxygen adsorption process. The change in the resistance is ca. 20%.

Figure 3 shows the electrical conductivity σ versus T for both the vacuum degassed and O_2 loaded (200 °C at 1 atm) ACF samples. After oxygen is admitted at 200 °C in 1 atm, the σ versus T curve is measured during cooling down to $T \sim 85$ K, which is close to the condensation temperature of oxygen (90 K). At $T \sim 85$ K, the excess O_2 is removed by vacuum pumping and the sample is further subjected to cooling by inserting the dip sample tube in liquid He. By plotting the data as log [σ] versus T^{-n}, we find nearly linear behavior for $n = 1/2$, as shown in figure 3(b). Taking into account the three-dimensionality of the nanographite network, the linear $T^{-1/2}$ is caused by variable range hopping with Coulomb blockade, reflecting the charging energy of nanographite domains in the carrier transport process [16, 17]. In this conduction model, the

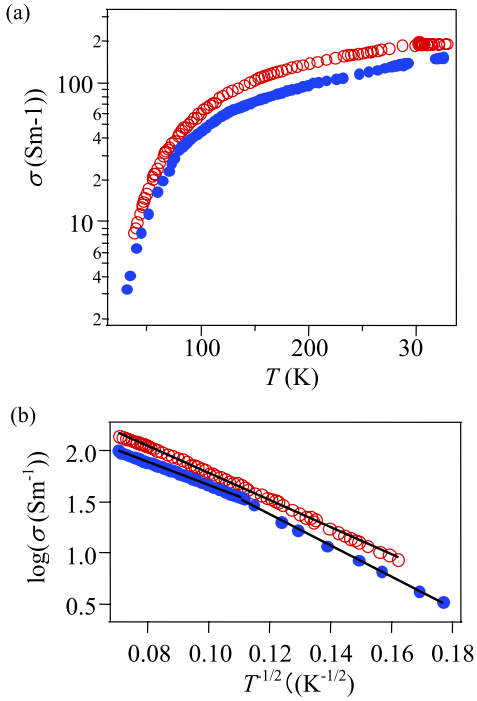

Figure 3. (a) Electrical conductivity (σ) versus T for the vacuum degassed and oxygen loaded single ACF (200 °C at 1 atm). (b) The conductivity re-plotted as $\log[\sigma]$ versus $T^{-1/2}$. The solid linear lines are fits with equation (1).

temperature dependence of the conductivity is represented by

$$\sigma = \sigma_0 \exp[-(T_0/T)^{1/2}] \quad (1)$$

$$T_0 = (6e^2/\pi k_B)[1/4\pi\varepsilon_r\varepsilon_0](1/\zeta) \quad (2)$$

where σ_0, ε_r, ε_0, ζ are, respectively, the conductivity at $T = \infty$, the dielectric constant of the medium surrounding the metallic islands, the permittivity of vacuum and the localization length. From the slope of the $\log[\sigma]$ versus $T^{-1/2}$ plot, we determine T_0 to be 730 K for the degassed ACFs. Assuming $\varepsilon_r = 10$ [17], the localization length ζ is estimated to be ca. 3 nm, which is almost the same as the mean in-plane size of the nanographene sheet. This suggests that the extended states of the carriers are confined within a single nanographite domain and hopping events between nanographite domains are subjected to the charging effects of nanographite domains.

In figure 3(b), the data for the O_2 doped sample shows two linear regimes, below and above $T \sim 70$ K. It is considered that this discontinuity of the conductivity at $T \sim 70$ K is associated with the formation of a condensed state of adsorbed oxygen molecules, as the condensation temperature of oxygen molecules is 90 K. Above 70 K, the fitting gives an estimate of $T_0 = 580$ K. The lowering of T_0 from that for the degassed ACF can be explained by the increase in the dielectric constant in the medium upon the occupation of the nanopores by oxygen molecules ($\varepsilon_r = 1.511$).

Figure 4 shows the temperature dependence of the TEP (S) for the vacuum degassed and O_2-loaded (200 °C, 1 atm) single ACF. The TEP value for the degassed sample remains

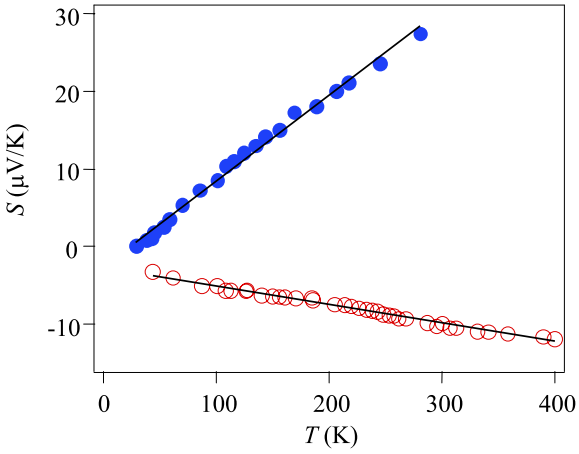

Figure 4. TEP (S) versus T for a single ACF vacuum degassed (200 °C) (open circle) and O_2-loaded (200 °C, 1 atm) (full circle). Solid lines are the fits to equation (5).

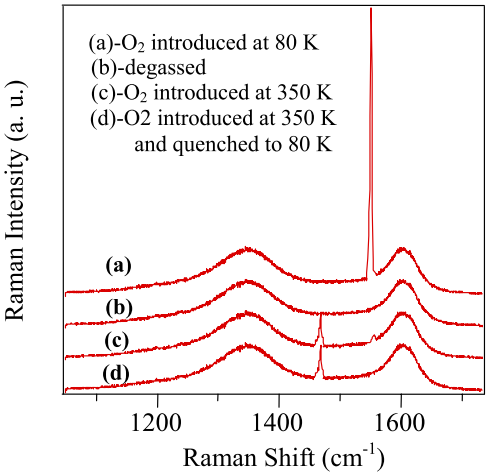

Figure 5. Raman scattering spectra of (a) ACFs with condensed phase O_2 when admitted at 80 K, (b) degassed ACFs, (c) after O_2 loading at 4 atm at 350 K, (d) after quenching to 80 K while pumping after the measurement of (c).

negative, with electron carriers over the whole temperature range, while that of the O_2-loaded sample remains positive, with hole carriers. In both cases, the TEP is almost linear with temperature, suggesting the presence of metallic conduction carriers. However, the simple linear temperature dependence without low temperature anomalies is in contrast with the results for bulk graphite, where the phonon drag effects introduce humps in the $S(T)$ curve [18, 19]. In the present system, the structural disorder and the small size of the nanographite domains suppress the phonon drag enhancement usually expected in a graphitic carbon system, that is, the phonon heat current is suppressed due to structural disorder. The scattering from domain boundaries probably provides the dominant scattering mechanism for the free carriers within a domain. Therefore, the linear behavior extending all the way from 10 to 400 K can be understood.

Figure 5 shows the Raman spectra for the degassed ACFs and the O_2-loaded sample that was exposed to O_2 at 350 K at 4 atm. Also, the spectrum of the sample O_2-loaded at 350 K

and quenched to 80 K while O_2 in the gas phase was pumped out, and that of the sample when O_2 was simply admitted at 80 K are given. The Raman spectrum for the degassed ACF (b) shows two broad bands near 1360 and 1590 cm^{-1}, which are the general first-order features for disordered graphitic carbons. The peak around 1590 cm^{-1} corresponds to the Raman allowed E_{2g} mode G-band in graphite. The D-band around 1360 cm^{-1} is absent in the spectra of bulk regular graphite, but becomes Raman-active in finite-size crystallites. The spectrum for the ACFs in equilibrium with O_2 at 4 atm at 350 K (c) shows two new bands not seen in the degassed ACFs; one at ∼1556 cm^{-1}, which is anticipated for the frequency of the gas-phase stretching mode of O_2, and another at ∼1468–1470 cm^{-1}, which is associated with the O_2 molecule downshifted by ∼100 cm^{-1} from the gas-phase stretching mode frequency. Since the 1556 cm^{-1} band disappears during pumping (d) and is present in the sample with solid O_2 at 80 K (a), it is concluded that this band is assigned to the gaseous O_2 and the weakly physisorbed O_2. Also, we can rule out the possibility that the 1468–1470 cm^{-1} band could be associated with another isotope of O_2, such as $^{16}O^{17}O$ etc. The $^{16}O^{18}O$ isotope has a band near 1480 cm^{-1}, but the abundance of these species relative to the $^{16}O^{16}O$ is <0.001%. Thus the possibility of isotope contamination can be excluded, and we can assign it to the chemisorbed O_2 molecules whose stretching mode is down shifted through interaction with the host nanographene sheet. In figure 6(a), we show an enlargement of the spectral region in the vicinity of the chemisorbed O_2 as the temperature is varied from 80 to 300 K while pumping on the cell. The spectra become intensified as the temperature is lowered. In the spectra at low temperatures (80–150 K), a weak feature is observed at 1466 cm^{-1}, on the low wavenumber side of the main peak. This suggests that a trace of oxygen molecules are more strongly chemisorbed to the host nanographene sheets.

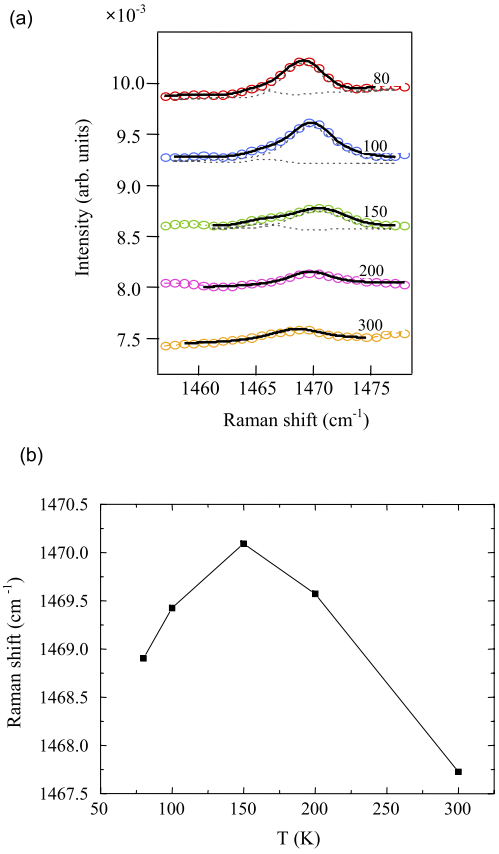

Figure 6. (a) Raman spectra of the stretching mode of chemisorbed O_2 taken as the sample is on a warming cycle from 80 to 300 K. The dotted lines are the deconvolution of the spectra into two components. (b) Temperature dependence of the Raman shift (main peak) of the chemisorbed O_2.

4. Discussion

Let us start the discussion with the kinetics of the heat-induced change and the oxygen adsorption process taking place at 200 °C. According to the experimental results shown in figure 2, the exponential decays in the desorption and oxygen adsorption processes have the characteristic relaxation times of $\tau_{Sd} = 3.2$ and $\tau_{Sa} = 26.7$ h, respectively, for the thermoelectric power, and $\tau_{Rd} = 6.2$ and $\tau_{Ra} = 12.3$ h, respectively, for the resistance change. The relaxation time for the desorption is shorter than that for the adsorption of oxygen in the change of TEP and resistance. Moreover, the difference in the relaxation times between the desorption and adsorption processes is more pronounced in the TEP data than in the resistance data. Another interesting feature is that the relaxation time is shorter in the TEP than the resistance data in the desorption process, whereas the trend is the opposite in the oxygen adsorption process. The results of TPD and TG/DTA demonstrate that the desorption process in vacuum at 200 °C is associated with the decomposition of functional groups, mainly carboxyl group, weakly bonded to the nanographene edges, while strongly bonded functional groups such as carbonyl and phenol groups remain still bonded.

The experimental finding that the relaxation time in the oxygen adsorption is considerably longer than that for the desorption implies that the oxygen adsorption proceeds along a route different from the reverse of the desorption process. Furthermore, the difference in the relaxation times between the TEP and the resistance change suggests that different physical quantities, having unique relaxation times, are responsible for the time dependence of the TEP and resistance change. In connection with this, the relation between the resistance and TEP is given in the following equation;

$$S = \frac{\sum_i \sigma_i S_i}{\sum_i \sigma_i} = \frac{\sigma_e S_e + \sigma_h S_h}{\sigma_e + \sigma_h} = \frac{n_e e\mu_e S_e + n_h e\mu_h S_h}{n_e e\mu_e + n_h e\mu_h} = \frac{-n_e e\mu_e |S_e| + n_h e\mu_h |S_h|}{n_e e\mu_e + n_h e\mu_h}, \quad (3)$$

where σ_i and S_i are the conductivity and TEP of the carrier i, respectively. In the case of the coexistence of electron and hole carriers, the TEP is described by carrier concentrations n_e, n_h, mobilities μ_e, μ_h, and TEP components $S_e(<0)$, $S_h(>0)$, for the electron and hole carriers. Assuming that the relaxation times for the TEP and resistance change are the same for the electron and hole carriers, equation (3) can be rewritten as

$$S = \frac{\sigma_e S_e + \sigma_h S_h}{\sigma_e + \sigma_h} \propto \frac{\exp(-t/\tau_S)\exp(-t/\tau_R)}{\exp(-t/\tau_R)} = \exp(-t/\tau_S), \quad (4)$$

where τ_S and τ_R are the relaxation times for the TEP and resistance/conductivity change, respectively. This means that the relaxation process in the TEP is governed by the energy dispersions of the electron and hole bands, which contribute to the TEP, whereas that for the resistance change is due to the carrier concentrations and mobilities. In addition, taking into account the opposite signs of electron and hole carriers in the TEP in equation (3), the change in the TEP is sensitive to the change in carrier type, although the conductivity is related to the total concentration of the carriers regardless of the sign. Therefore, the steep drop in the TEP from positive to negative in the desorption process suggests that the change in the carrier type from hole to electron takes place in the early stage of the decomposition process, in the whole of which the total carrier concentration and mobilities vary with a longer relaxation time. In contrast, in the oxygen adsorption process, in which the relaxation time is longer in the TEP than the resistance change, the changes in the carrier concentration and mobilities take place earlier than that of the carrier type. What is different between the desorption and adsorption processes is relevant to the presence or absence of O_2 species. In the desorption process, no O_2 molecule is observed, as evidenced by the TPD experiment, whereas the Raman spectrum of the O_2 stretching mode demonstrates the presence of O_2 molecules adsorbed in the nanopores in the oxygen adsorption process. Eventually, the removal of oxygen-including functional groups from the well oxidized nanographene edges in the desorption process seriously affects the electronic state, resulting in the intense annihilation of hole carriers and creation of electron carriers. On the other hand, the adsorption of O_2 molecules proceeds at a moderate reaction rate with a slow relaxation time, accompanied by the creation of hole carriers through charge transfer from the constituent nanographene sheets to the O_2 molecules.

Next, we discuss the charge transfer in the oxygen adsorption process on the basis of the results of TEP and the Raman spectra of the O_2 stretching mode. The change in the sign of the TEP from negative to positive with the O_2 uptake, and the downshift of the O_2 stretching mode, demonstrate charge transfer from the nanographene sheets to the adsorbed O_2 molecules. Here, we first estimate the charge transferred to the adsorbed O_2 molecules. According to the literature, the O_2 adsorbed on the surface of a metal, such as Cu [20], Ag [21], etc, are subjected to charge transfer, where O_2 molecules show a downshift of the O–O stretching mode frequency in proportional to the amount of charge transferred to O_2, given by $\Delta\omega/\delta \sim 780\ \mathrm{cm}^{-1}/e$, where $\Delta\omega$ is the shift of the O–O stretching mode frequency and δ is the partial charge, defined as $O_2^{\delta-}$. Use of the shift of $\Delta\omega \sim 88\ \mathrm{cm}^{-1}$ ($=1556\ \mathrm{cm}^{-1} - 1468\ \mathrm{cm}^{-1}$) observed in the present experiment gives an estimate of $\delta \sim 0.11e/O_2$.

Let us observe the charge transfer from the side of nanographene using the results of the TEP. The linear TEP is typical of a diffusive thermoelectric power process [18, 19]. Variable range hopping with a Coulomb blockade was used to fit the $\sigma(T)$ data in the analysis. However, there is no appropriate expression in this limit for the TEP, in spite of some theoretical predictions [22, 23]. Here, we expect that the TEP will approximately follow the diffusive behavior of a nanographite domain and the hopping between domains will not contribute significantly to the T-behavior of the TEP. Accordingly, the electron diffusion term of the TEP is given by:

$$S = (\pi^2 k_B^2/3e)[(1+P)/E_F)]T \tag{5}$$

where k_B, e and E_F are the Boltzmann constant, the electronic charge and the Fermi energy, respectively. The parameter P represents the exponent in the power law energy dependence of the relaxation time of the carriers, given by $\tau = \tau_0 E^P$ [18, 19]. Fitting of the S versus T plot to equation (5) gives an estimate of $E_F \sim +0.1$ eV for the O_2 loaded system and $E_F \sim -0.3$ eV for the degassed system, on the assumption of $P = 0$ for simplicity. This finding suggests that the removal of oxygen-including functional groups at 200 °C shifts the Fermi energy up, giving rise to the creation of electron carriers, whereas the oxygen loading shifts it down, resulting in the creation of hole carriers. According to the 2D π band model, the charge transfer rate per carbon atom f_C (the number of charges per C atom) as a function of the Fermi energy E_F is given by:

$$f_C = \frac{E_F^2}{\sqrt{3}\pi\gamma_0^2} \tag{6}$$

where $\gamma_0 = 3.12$ eV is the intra-sheet transfer integral [6]. Using the calculated change in the Fermi energy $\Delta E_F \sim (0.1 - (-0.3))$ eV $= 0.4$ eV, we estimate the charge transfer rate for the O_2-loaded sample to be $f_C \sim 0.002$. However, when we discuss the issue on the charge transfer from the oxygen side, this estimate should be corrected in the present case since the edge states (singly occupied non-bonding π-electron state) at the Dirac point ($E_F = 0$) of nanographene/nanographite work as an electron reservoir [24–26]. The correction is given as $\delta_{ng} \sim N_{ng} f_C + N_{edge} = N_{ng}\langle f_C\rangle$, where δ_{ng}, N_{ng}, N_{edge}, and $\langle f_C\rangle$ are the charge per nanographene sheet, the total number of carbon atoms in an individual nanographene sheet, the number of zigzag edge carbon atoms having a non-bonding edge state in an individual nanographene sheet, and the mean charge transfer rate, respectively. According to previous work [17, 26], the concentration of the edge state spins is roughly estimated to be ~ 1 ($N_{edge} \sim 1$) for an individual nanographene sheet having a mean size of 3 nm, which involves ca. 300 carbon atoms ($=N_{ng}$). Hence, the charge on an individual nanographene sheet is estimated roughly as $\delta_{ng} \sim 1.6$.

Here, the relationship between the charge on the adsorbed O_2 molecule and the charge transfer rate from the carbon atom should be clarified, although it is considerably difficult to discuss it quantitatively since the total amount of oxygen molecules participating in the adsorption process cannot be estimated in the sample vacuum-heat-treated at 200 °C. Let us try to get a reasonable idea by a rough estimation of the number of oxygen atoms adsorbed in a nanographene sheet. According to previous work [12], the weight uptake in the oxygen adsorption at room temperature is estimated as ~ 3 mg/1 g of ACF. This corresponds to 0.3 O_2 molecule/nanographene sheet or ~ 1 O_2 molecule/nanographite domain (3–4 stacked nanographene sheets). Eventually, the charge on an O_2

molecule (δ) is obtained as $\delta \sim 5(\delta \sim \delta_{ng}/$ (number of adsorbed oxygen molecules/nanographene) $\sim$1.6/0.3). This is more than one order of magnitude larger than that estimated from the Raman spectra ($\delta \sim 0.1$) for the chemisorbed oxygen molecules. This large discrepancy is due to the simplicity of the model we employ in the analysis of the TEP. In addition, each nanographite domain is assumed to be occupied by only one oxygen molecule. More realistically, due to the disordered arrangement of nanographite domains in ACF, many of the nanographite domains in ACF are inaccessible to oxygen molecules, and many of the domains are over populated by oxygen molecules. However, we should note the difference in the experimental conditions between the previous work [12] and the present one. In the latter work, oxygen is loaded at 350 K at 4 atm, which is different from the oxygen adsorption under atmospheric conditions at room temperature in [12]. Therefore, the large discrepancy can be partly related to a large increase in the concentration of O_2 molecules in the present experiment, which is carried out under more extreme conditions, even though the simplicity of the model still remains a serious issue. Experiments on the oxygen adsorption isotherm with well heat-treated samples, and the same condition as the present experiment, are required in the future to clarify this issue, in addition to the improvement of the analysis of the TEP.

Finally, we comment on the temperature dependence of the Raman shift of the stretching mode of chemisorbed O_2 molecules. According to the experimental result shown in figure 6(b), the peak position is shifted up as the temperature is lowered from 300 to ca. 150 K, and then becomes less temperature dependent below ca. 150 K. The previous work [5] indicates that the feature of O_2 adsorption is changed between the low and high temperature regimes, with a crossover temperature of 100–200 K. In the low temperature regime, the physisorption phenomenon governs, while chemisorption is activated successively upon the elevation of temperature to the high temperature range. The downshift related to the increase in the charge transfer rate in the high temperature regime is associated with the activation of chemisorption upon the elevation of the temperature. The less temperature dependent feature in the Raman shift in the low temperature regime can be explained by assuming that the state of the chemisorbed O_2 molecules is quenched.

5. Conclusion

The adsorption/desorption processes of oxygen is investigated in nanoporous carbon (ACFs) consisting of a disordered network of nanographene sheets. The heat-induced desorption at 200 °C shows the decomposition of oxygen-including functional groups, such as carboxyl groups weakly bonded to nanographene edges, while the strongly bonded functional groups, such as carbonyl and phenol, remain bonded. The removal of the weakly bonded functional groups having negative charges brings about the change in the type of majority carriers from holes to electrons through back charge transfer from the functional groups to the nanographene sheets. The oxygen adsorption after the desorption at 200 °C brings ACF back to the electronic state with holes being the majority carriers. In this process, a large concentration of negatively charged $O_2^{\delta-}$ molecules ($\delta \sim 0.1$) are created through charge transfer from the nanographene sheets to the adsorbed oxygen molecules. The changes in the thermoelectric power and electrical resistance in the desorption process are steeper than those in the oxygen adsorption process. This suggests the irreversibility between the desorption process and the adsorption process; the former is the heat-induced decomposition process of the well oxidized nanographene edges and the latter is the O_2 chemisorption to the less oxidized edges accompanied by the creation of negatively charged O_2 molecules. It is concluded that the removal of weakly covalent-bonded oxygen-including groups has a stronger effect on the electronic structure of the nanographene sheet than the interaction of negatively charged O_2 molecules chemisorbed with charge transfer interaction with nanographene sheets.

The issue of the interaction between graphene edges and oxygen is extremely important not only for basic physical chemistry but also for practical applications. In order to comprehensively understand the interaction between nanographene, particularly its edge, and oxygen molecules, more detailed investigations are necessary in the extended temperature range up to $\sim$1000 °C, in which we can expect a variation of functional groups from oxygen-including ones to hydrogen.

Acknowledgments

The authors in the Pennsylvania State University group were supported by the Penn State MRSEC (DMR-0213623). The authors in the Tokyo Institute of Technology group were supported by the Grant-in-Aid for Scientific Research No. 20001006 from the Ministry of Education, Culture, Sports, Science and Technology, Japan.

References

[1] Kanoh H and Kaneko K 1996 *J. Phys. Chem.* **100** 755
[2] Kaneko K 2000 *Carbon* **38** 287
[3] Suzuki M 1994 *Carbon* **32** 577
[4] Otake Y and Jenkins R G 1993 *Carbon* **31** 109
[5] Joseph Joly V L, Takai K and Enoki T 2009 *J. Phys. Chem. Solids* at press
[6] Enoki T, Suzuki M and Endo M 2003 *Graphite Intercalation Compounds and Applications* (New York: Oxford University Press)
[7] Sugihara K, Takahara K, Takai K and Enoki T 2007 *Phys. Rev.* B **75** 205422
[8] Takahara K, Takai K, Enoki T and Sugihara K 2007 *Phys. Rev.* B **76** 0354422
[9] Dresselhaus M S, Fung A W P, Rao A M, di Vittorio S L, Kuriyama K, Dresselhaus G and Endo M 1992 *Carbon* **30** 1065
[10] Nakayama A, Suzuki K, Enoki T, Ishii C, Kaneko K, Endo M and Shindo M 1995 *Solid State Commun.* **93** 331
[11] Sugihara K, Nakayama A and Enoki T 1995 *J. Phys. Soc. Japan* **64** 2614

[12] Kobayashi N, Enoki T, Ishii C, Kaneko K and Endo M 1998 *J. Chem. Phys.* **109** 1983
[13] Sato H, Kawatsu N, Enoki T, Endo M, Kobori R, Maruyama S and Kaneko K 2003 *Solid State Commun.* **125** 641
[14] Sumanasekera G U, Grigorian L and Eklund P C 2000 *Meas. Sci. Technol.* **11** 273
[15] Eklund P C and Mabatah A K 1977 *Rev. Sci. Instrum.* **48** 775
[16] Fung A W P, Dresselhaus M S and Endo M 1993 *Phys. Rev.* B **48** 14953
[17] Shibayama Y, Sato H, Enoki T, Bi X X, Dresselhaus M S and Endo M 2000 *J. Phys. Soc. Japan* **69** 754
[18] Tsuzuku T and Sugihara K 1975 *Chemistry and Physics of Graphite* vol 12 (New York: Dekker) p 109
[19] Enoki T, Sakamoto N, Nakazawa K, Suzuki K, Sugihara K and Kobayashi K 1993 *Phys. Rev.* B **47** 10662
[20] Prabhakaran K, Sen P and Rao C N R 1986 *Surf. Sci.* **177** L971
[21] Prabhakaran K and Rao C N R 1987 *Surf. Sci.* **186** L575
[22] Burns M J and Chaikin P M 1985 *J. Phys. Solid State Phys.* **18** L743
[23] Parfenov O E and Shklyaruk F A 2007 *Semiconductors* **41** 1021
[24] Fujita M, Wakabayashi K, Nakada K and Kusakabe K 1996 *J. Phys. Soc. Japan* **65** 1920
[25] Enoki T, Kobayashi Y and Fukui K 2007 *Int. Rev. Phys. Chem.* **26** 609
[26] Enoki T and Takai K 2009 *Solid State Commun.* **149** 1144